Functional Suppression of HAMP Domain Signaling Defects in the *E. coli* Serine Chemoreceptor

Run-Zhi Lai and John S. Parkinson

Biology Department, *University of Utah, Salt Lake City, UT 84112, USA*

Correspondence to John S. Parkinson: *University of Utah, 257 South 1400 East, Salt Lake City, UT 84112, USA.*
parkinson@biology.utah.edu
http://dx.doi.org/10.1016/j.jmb.2014.08.003
Editor by B. Poolman

Abstract

HAMP domains play key signaling roles in many bacterial receptor proteins. The four-helix HAMP bundle of the homodimeric *Escherichia coli* serine chemoreceptor (Tsr) interacts with an adjoining four-helix sensory adaptation bundle to regulate the histidine autokinase CheA bound to the cytoplasmic tip of the Tsr molecule. The adaptation helices undergo reversible covalent modifications that tune the stimulus-responsive range of the receptor: unmodified E residues promote kinase-off output, and methylated E residues or Q replacements at modification sites promote kinase-on output. We used mutationally imposed adaptational modification states and cells with various combinations of the sensory adaptation enzymes, CheR and CheB, to characterize the signaling properties of mutant Tsr receptors that had amino acid replacements in packing layer 3 of the HAMP bundle and followed *in vivo* CheA activity with an assay based on Förster resonance energy transfer. We found that an alanine or a serine replacement at HAMP residue I229 effectively locked Tsr output in a kinase-on state, abrogating chemotactic responses. A second amino acid replacement in the same HAMP packing layer alleviated the I229A and I229S signaling defects. Receptors with the suppressor changes alone mediated chemotaxis in adaptation-proficient cells but exhibited altered sensitivity to serine stimuli. Two of the suppressors (S255E and S255A) shifted Tsr output toward the kinase-off state, but two others (S255G and L256F) shifted output toward a kinase-on state. The alleviation of locked-on defects by on-shifted suppressors implies that Tsr-HAMP has several conformationally distinct kinase-active output states and that HAMP signaling might involve dynamic shifts over a range of bundle conformations.

Introduction

Motile prokaryotes use transmembrane chemoreceptors known as methyl-accepting chemotaxis proteins (MCPs) to sense and track chemical gradients in their environments [1]. Extensive studies of chemotactic behavior in *Escherichia coli* have elucidated the basic mechanisms of MCP signaling [2]. Four MCPs of *E. coli*—Tar (aspartate and maltose sensing), Tsr (serine), Tap (dipeptides and pyrimidines), and Trg (ribose, galactose, and glucose)—have similar functional architectures (Fig. 1a): an overall homodimeric organization, a periplasmic ligand-binding domain, and a cytoplasmic signaling domain. MCPs communicate stimulus information to the cell's flagellar motors by forming stable ternary complexes with CheA, a histidine autokinase, and CheW, which couples CheA activity to receptor control. CheA activity, in turn, controls phosphorylation of CheY, which modulates the direction of flagellar rotation. Counterclockwise rotation, the default condition, produces forward swimming; phospho-CheY promotes clockwise rotational episodes that randomize cell heading. CheZ, a dedicated phosphatase, ensures that phospho-CheY is short-lived so that the cell can respond quickly to changes in chemoeffector levels.

A HAMP domain, located at the cytoplasmic face of the cell membrane, plays a central role in transmitting conformational changes between the sensing and signaling portions of the chemoreceptor (Fig. 1a) [3]. The remainder of the MCP cytoplasmic domain comprises a long, antiparallel, four-helix, coiled-coil bundle, with CheA and CheW binding determinants at its hairpin tip and sensory adaptation sites near its connections to HAMP (Fig. 1a) [2,4].

Changes in chemoattractant occupancy at the periplasmic sensing domain cause inward displacements of a transmembrane helix (TM2) adjoining HAMP [5]. The asymmetric piston input to HAMP in turn promotes conformational changes that down-regulate CheA kinase activity. Subsequent covalent modifications at the adaptation site residues terminate the signaling response by opposing HAMP-induced conformational changes at the kinase control tip and by shifting ligand affinity to attenuate stimulus input [6]. Two MCP-specific enzymes, CheR, a glutamic acid (E) methyltransferase, and CheB, a glutamyl methyl ester (Em) methylesterase and glutamine (Q) deamidase, control adaptational modification state. Methylation enhances CheA activity; demethylation and deamidation reduce CheA activity [6].

HAMP domains play prominent roles in a wide variety of bacterial signaling proteins, but how they mediate input–output communication is not yet clear [3,7]. The first high-resolution structure of a HAMP domain from Af1503, a thermophile protein, revealed a parallel, homodimeric, four-helix bundle organization, comprising two amphiphilic helices (AS1 and AS2) and an intervening non-helical connector (CTR) from each subunit (Fig. 1b) [8]. Subsequent HAMP structures have exhibited the same overall organization but with variations in helix alignments and bundle-stabilizing contacts [9–11]. *In vitro* [12] and *in vivo* [13] crosslinking studies, as well as extensive genetic evidence [14–16], indicate that the HAMP domains in *E. coli* chemoreceptors most likely operate as parallel, four-helix bundles similar to the Af1503 HAMP structure.

Chemoreceptor signaling complexes can shift between two output modes, an "on" state (ON) with high CheA kinase activity and an "off" state (OFF) with essentially no kinase activity. Overall receptor output reflects the fraction of receptors in the ON and OFF states. Stimuli and adaptational modifications shift the two-state equilibrium to produce behavioral responses and subsequent sensory adaptation. Several models based on the four-helix bundle have been proposed to explain the structural nature of HAMP signaling states. The gearbox [8] and scissors [12] models invoke discrete HAMP conformations for the ON and OFF receptor signaling states. In contrast, the dynamic-bundle model proposes that the HAMP and methylation helix (MH) bundles have opposed packing stabilities and that the dynamic structural interplay between these two elements determines receptor signal output [3,15]. In the dynamic-bundle model, the kinase-on and kinase-off HAMP signaling states are not discrete structures, but rather dynamic ensembles of bundle conformations [16,17].

Residue A291 in the AS1 helix of Af1503 HAMP provided a key tenet for the gearbox model. Hulko *et al.* noted that an alanine at that position would favor "complementary *x-da*" packing of the HAMP helices, whereas bulkier, more hydrophobic residues should favor a more conventional, knobs-into-holes ("*a-d*") packing arrangement [8]. Because many HAMP domains have smaller, less hydrophobic residues at this position than at other bundle-packing positions, Hulko *et al.* suggested that this core residue serves to poise the HAMP bundle between the *a-d* and *x-da* packing alternatives, thereby facilitating signal state ("gearbox") transitions [8]. Subsequent structure–function studies of chimeric Af1503 signaling

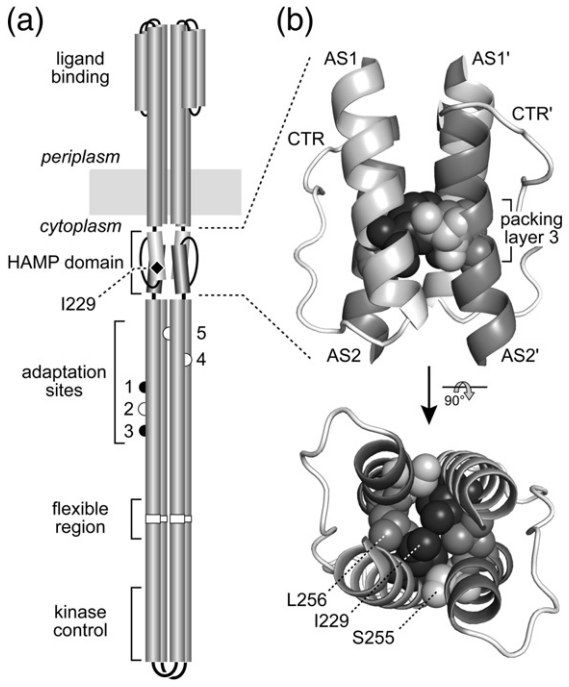

Fig. 1. Architectural landmarks in the Tsr molecule. (a) Cartoon of the Tsr homodimer. Cylindrical segments represent α-helical regions, drawn approximately to scale. Adaptation sites: white circles represent native glutamate residues that are direct substrates for CheR-mediated methylation; black circles indicate glutamine residues that must be deamidated by CheB before they can be methylated by CheR. The flexible region, defined by conserved glycine hinge residues (white boxes), transmits conformational changes between the adaptation helix bundle and the receptor tip, where CheW and CheA bind to form ternary signaling complexes. The HAMP domain relays stimulus-induced conformational changes to the adaptation bundle to control receptor signal output. The black diamond indicates the position of Tsr residue I229, the principal subject of the present study, in the AS1 helix. (b) Structure of the Tsr HAMP domain modeled from the atomic coordinates of Af1503 HAMP [8]. Each HAMP subunit contains 46 residues (L218–L263), comprising two helices (AS1 and AS2) joined by a non-helical connector (CTR). The four HAMP helices in the Tsr homodimer form a parallel, coiled-coil bundle with four layers of hydrophobic packing residues. Side-chain atoms of layer 3 residues I229, S255, and L263 are spacefilled to indicate their probable packing arrangement.

proteins have been interpreted as consistent with this idea [11,18]. However, *E. coli* chemoreceptors have an isoleucine residue at this key HAMP packing position. Do the HAMP domains in MCP molecules operate differently?

A mutant Tsr receptor that has an alanine replacement at residue I229, the counterpart to A291 of Af1503 HAMP, cannot promote serine chemotaxis [15,16]. Second-site mutations that create an amino acid replacement at AS2 residue S255 or L256 in the same hydrophobic packing layer of the Tsr-HAMP bundle (Fig. 1b) can suppress the I229A functional defect, implying proper HAMP conformational control in the doubly mutant receptors [15]. In principle, these suppression effects could lend support to either the discrete conformation or dynamic ensemble HAMP signaling models. To distinguish mechanistic predictions of the two models, we measured, using a Förster resonance energy transfer (FRET)-based *in vivo* kinase assay [19], the signaling properties of singly and doubly mutant Tsr receptors that had amino acid replacements in Tsr-HAMP packing layer 3 (Fig. 1b).

Results

Chemotactic behavior of Tsr-I229 mutants and their suppressors

Alanine and serine replacements at Tsr residue I229 shift output toward the CW signaling state, consonant with high kinase activity [16], and abrogate chemotaxis in tryptone semi-solid agar assays [15]. Certain amino acid replacements at residues S255 and L256 in the same bundle-packing layer of HAMP (Fig. 1b) suppress the chemotaxis defects of Tsr-I229A and Tsr-I229S [15]. We selected four suppressor alleles (S255A, S255E, S255G, and L256F) for the present study and verified their phenotypes by introducing plasmid pPA114 derivatives bearing singly or doubly mutant *tsr* genes into receptor-less host strain UU2612. On semi-solid tryptone medium, which contains approximately 670 μM serine [20], all suppressor and doubly mutant receptors supported chemotactic responses similar to that of wild-type Tsr. Results for Tsr-I229A are shown in Fig. 2; Tsr-I229S behavior was similar (data not shown).

To estimate the detection thresholds of the serine-responsive Tsr variants, we examined their ability to promote chemotaxis on minimal semi-solid agar medium containing 4, 20, or 100 μM serine (Fig. S1). Tsr-S255A and Tsr-S255E responded to 4 μM serine, as did wild-type Tsr. In contrast, Tsr-S255G had a response threshold at 20 μM serine and Tsr-L256F only responded at 100 μM serine. The S255G and L256F changes evidently reduce the serine sensitivity of Tsr. None of the doubly mutant receptors produced a chemotactic response at 100 μM serine (Fig. S1 and data not shown), suggesting that their detection thresholds are higher than those of wild-type Tsr and its singly mutant suppressor variants.

In vivo assay of receptor-coupled CheA kinase activity

Tsr-I229A and Tsr-I229S suppression patterns are allele specific, implying that restoration of signaling function occurs through compensatory conformational changes that restore more normal structure or packing stability to the HAMP bundle [15]. To determine the functional basis for those suppression effects and to gain insights into their possible structural basis, we characterized mutant Tsr receptors with a FRET-based *in vivo* kinase assay developed by Sourjik and Berg [19]. The assay measures CheA activity-dependent interactions between CFP-tagged CheZ (the FRET donor) and YFP-tagged CheY (the FRET acceptor). Phosphorylation of CheY enhances its affinity for the CheZ

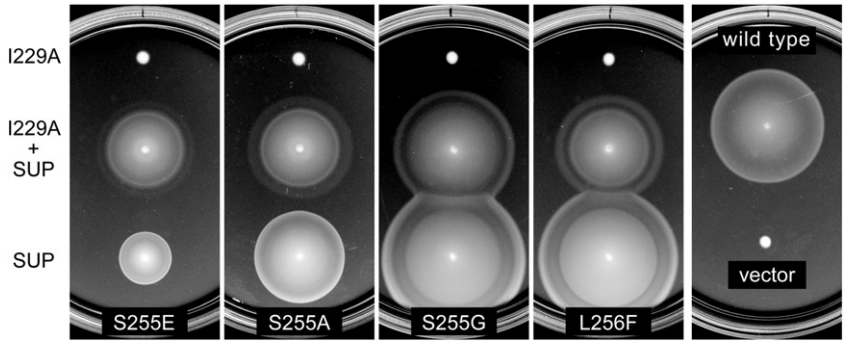

Fig. 2. Chemotaxis phenotypes of Tsr-HAMP mutants. Colony morphologies on tryptone soft agar plates of UU2612 cells carrying plasmid pPA114 derivatives with the indicated Tsr-HAMP lesions. Plates contained 0.27% agar and were incubated at 32.5 °C for 7.5 h.

phosphatase, promoting an increase in CheY–CheZ complexes and in the FRET signal. Thus, the assay reports on CheA autophosphorylation activity, which is under receptor control and the rate-limiting step in phosphorylation of CheY. To assess the signaling properties of mutant receptors, we expressed them from the salicylate-regulatable pPA114 plasmid. The CheY-YFP/CheZ-CFP FRET reporters were expressed from a compatible, IPTG-regulatable plasmid (pVS88). Plasmid pairs were transferred into FRET reporter strains deleted for the chromosomal *cheY* and *cheZ* loci and for all five *E. coli* MCP family receptor genes, enabling us to follow CheA activity changes in the cells in response to serine stimuli. The dose–response data were fitted to a multisite Hill equation to obtain values for $K_{1/2}$, the serine concentration that inhibited 50% of CheA kinase activity, and the Hill coefficient, a measure of response cooperativity.

Signaling properties of mutant receptors in the absence of sensory adaptation

In UU2567, a FRET reporter strain lacking the CheR and CheB enzymes of the sensory adaptation system, receptor molecules remain unmodified, undergoing neither methylation nor deamidation/demethylation reactions. Under these conditions, wild-type Tsr molecules have a QEQEE residue pattern at adaptation sites 1–5. E residues represent the unmethylated state and shift receptor output to lower kinase activity; Q residues mimic the methylated (Em) state and shift receptor output to higher kinase activity. In the QEQEE (2-Q) modification state, only wild-type Tsr and the S255A and S255G mutant receptors responded to serine (Fig. 3 and Table S1). Tsr-S255A had a $K_{1/2}$ of about 3 μM, considerably lower than that of wild-type Tsr (~17 μM), indicating a shift toward the OFF state. In contrast, Tsr-S255G had a much higher than wild-type serine threshold ($K_{1/2}$ ~ 1600 μM), indicating an output shift toward the ON state.

To determine the signaling propensities of the other mutant receptors in strain UU2567, we mutationally altered adaptation sites 1–4 to mimic different modification states, ranging from EEEEE (0-Q) to QQQQE (4-Q). The fifth adaptation site in Tsr (E502) [21,22] was maintained as E for these experiments. Each receptor with a suppressor change responded over a subset of modification states, allowing us to classify its signaling shift. Tsr-S255A responded with increasing thresholds over the 2-, 3-, and 4-Q states, confirming its off-biased nature. Tsr-S255G responded with increasing thresholds over the 0-, 1-, and 2-Q states, confirming its on-biased nature. Tsr-S255E only responded in the 3- and 4-Q states, consistent with extreme off-biased output, whereas Tsr-L256F only responded in the 0- and 1-Q states, consistent with extreme on-biased output (Fig. 3). Tsr-I229A and Tsr-I229S did not respond to serine at any modification state (Table S1). In principle, these mutant

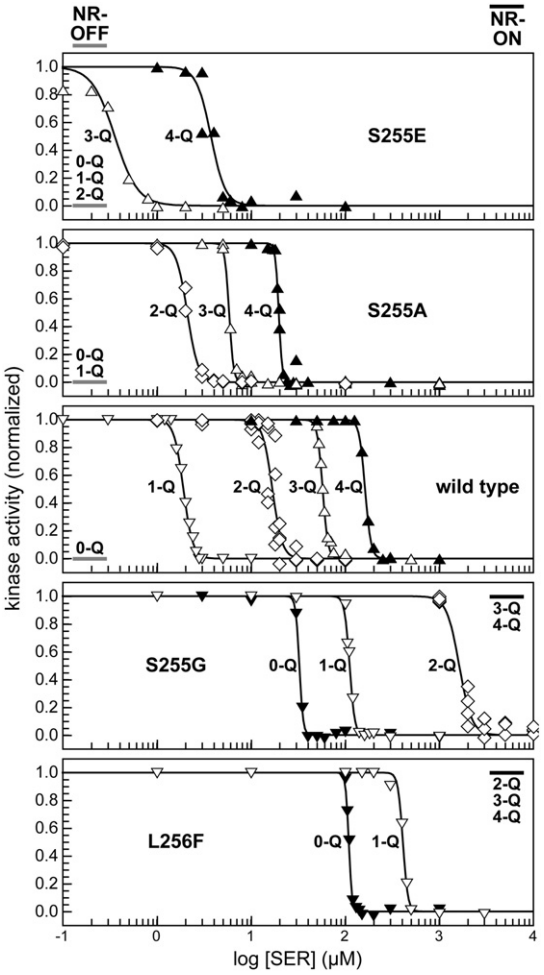

Fig. 3. Signaling properties of Tsr-HAMP mutant receptors in the absence of sensory adaptation enzymes. Panels show serine dose–response behaviors of UU2567 cells ($CheR^-$ $CheB^-$) carrying plasmid pPA114 derivatives expressing mutant Tsr receptors with different combinations of Q and E residues at adaptation sites 1–4. Modification variants were as follows: 0-Q, EEEEE (filled down-triangle); 1-Q, EEQEE (open down-triangle); 2-Q, QEQEE (open diamond); 3-Q, QQQEE (open up-triangle); 4-Q, QQQQE (filled up-triangle). Nonresponsive Q-state variants of particular receptors are listed in the lower left (NR-OFF, no serine response and no kinase activity) or upper right (NR-ON, no serine response but with high kinase activity) of each panel. Data from one or more independent *in vivo* FRET kinase experiments (see Materials and Methods) for each Q-state variant of a mutant receptor were jointly fitted to a Hill equation to illustrate the reproducibility of the measurements. Individual Hill fits for each experiment were averaged to obtain mean ± standard error values for $K_{1/2}$ (Table S1) and Hill coefficient (Table S2).

receptors could be locked in either a kinase-on or a kinase-off signaling state. Doubly mutant receptors containing the I229A lesion in combination with each of the suppressors also failed to respond over 1- to 4-Q modification states (Table S1). However, in the EEEEE state, they showed very high serine response thresholds (1–10 mM), suggesting that I229A causes an extreme shift toward the ON state that dominates the signaling behavior of the doubly mutant receptors.

Measuring the kinase activities of locked-output receptors

The kinase activity of serine-responsive receptors can be calculated from their maximal FRET change to a saturating stimulus [23]. To determine the kinase activities produced by Tsr-I229A and other nonresponsive receptors, we monitored changes in their FRET signals after KCN treatment. Cyanide is a potent inhibitor of cytochrome oxidase in the respiratory chain and rapidly collapses cellular proton motive force and ATP levels [24]. Because ATP is the phosphodonor for CheA autophosphorylation, we reasoned that KCN should elicit an attractant-like FRET response from a locked-on receptor but no FRET change from a locked-off receptor. Comparisons of CheA kinase activity measurements by the serine and KCN methods validated this approach. For example, wild-type Tsr in the 4-Q modification state showed comparable FRET responses to a saturating serine stimulus and to treatment with 3 mM KCN (pH 7.0), whereas Tsr-L256F (4-Q), which should be locked in the on state (Fig. 3 and Table S1), failed to respond to serine but showed a KCN response indicative of high kinase activity (Fig. S2). Tsr-L256F (0-Q) showed substantial serine and KCN FRET responses, whereas wild-type Tsr (0-Q) did not respond to either serine or KCN, consistent with locked-off behavior in this modification state (Fig. S2 and Table S1).

We used the KCN method to determine whether unresponsive receptors had locked-on or locked-off outputs. Tsr-I229A showed no serine response in any modification state but high kinase activity throughout the 0-4 Q range (Fig. 4 and Table S3), properties consistent with locked-on output. In combination with any of the four suppressors, Tsr-I229A still exhibited high kinase activities in all modification states (Fig. 4 and Table S3). Tsr-I229S, although tested at fewer modification states, showed behavior similar to that of Tsr-I229A (Table S3). The on-shifted S255G and L256F receptors showed high kinase activities at all modification states (Fig. 4 and Table S3), consistent with locked-on outputs at high-Q modification states. The off-shifted S255E and S255A receptors, on the other hand, showed locked-off behavior at low-Q modification states (Fig. 4 and Table S3). Lastly, wild-type Tsr showed no kinase activity in the 0-Q state but high kinase activities in all other states (Fig. 4 and Table S3). In summary, all receptors produced either very low or comparably high kinase activities in strain UU2567, which lacks the sensory adaptation enzymes. Previous *in vivo* studies have also reported maximal kinase activity over a range of receptor response thresholds [22,25,26], whereas this is not the typical case for *in vitro* studies of receptor signaling [27,28].

Sensory adaptation effects on the signaling properties of mutant receptors

The functional suppression effects observed in soft agar chemotaxis assays only occur in adaptation-proficient host strains (Fig. 2 and data not

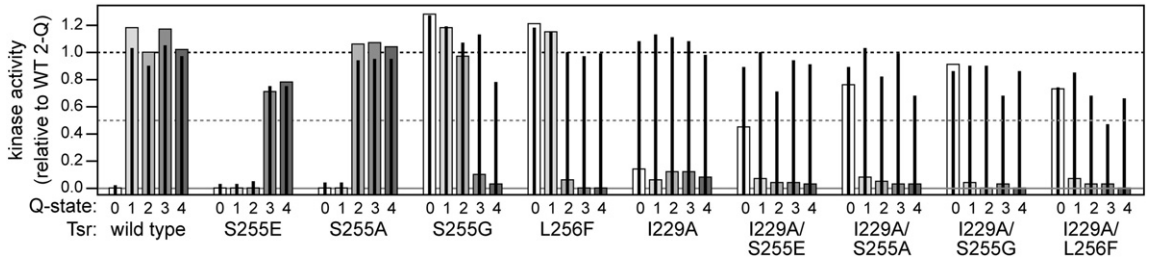

Fig. 4. CheA kinase activities of mutant Tsr signaling complexes. Kinase activities promoted by plasmid pPA114-encoded mutant receptors were measured by *in vivo* FRET assays in strain UU2567 ($CheR^-$ $CheB^-$). Histogram bars indicate activities calculated from the FRET change elicited by a saturating serine stimulus (or, if no evident response, to 10 mM serine). Black vertical lines indicate kinase activities calculated from the FRET change elicited by 3 mM KCN. Five Q/E modification states of each mutant receptor were tested: 0-Q, EEEEE (white bars); 1-Q, EEQEE (light gray); 2-Q, QEQEE (gray); 3-Q, QQQEE (dark gray); 4-Q, QQQQE (very dark gray). All kinase activities were normalized to that of Tsr wild type in the 2-Q state and are listed in Table S3. Broken lines at 0.5 and 1.0 relative activities are included solely to facilitate comparisons among and between the receptor mutants. Note that the scale begins below 0.0 to identify the mutants with near-zero values.

shown), implying that the CheR and CheB sensory adaptation enzymes can shift the mutant receptors into a physiologically relevant response range. To quantify the effects of sensory adaptation on mutant receptor signaling, we introduced plasmid pPA114 derivatives into FRET reporter strain UU2700 (CheR$^+$ CheB$^+$). The four Tsr suppressor variants exhibited sensitive serine responses in this strain (Fig. 5). The response thresholds of Tsr-S255A, Tsr-S255E, and Tsr-S255G were quite similar to that of wild-type Tsr ($K_{1/2}$ ~ 0.5 μM); the more extreme on-biased L256F receptor was somewhat less sensitive ($K_{1/2}$ ~ 7.5 μM) (Fig. 5 and Table S1). Although Tsr-I229A became serine responsive in the adaptation-proficient host, its detection threshold was quite high ($K_{1/2}$ ~ 450 μM) (Fig. 5). Tsr-I229S showed similar behavior (Table S1 and Fig. S3). The suppressors lowered the high response thresholds of the I229A receptor (Fig. 5) and the I229S receptor (Table S1 and Fig. S3). The detection sensitivities of the doubly mutant receptors were intermediate to those of the component singly mutant receptors but not strictly additive. For example, S255E, the most off-biased of the suppressors, produced the smallest threshold shifts for the on-biased I229A (Fig. 5) and I229S (Table S1 and Fig. S3) receptors.

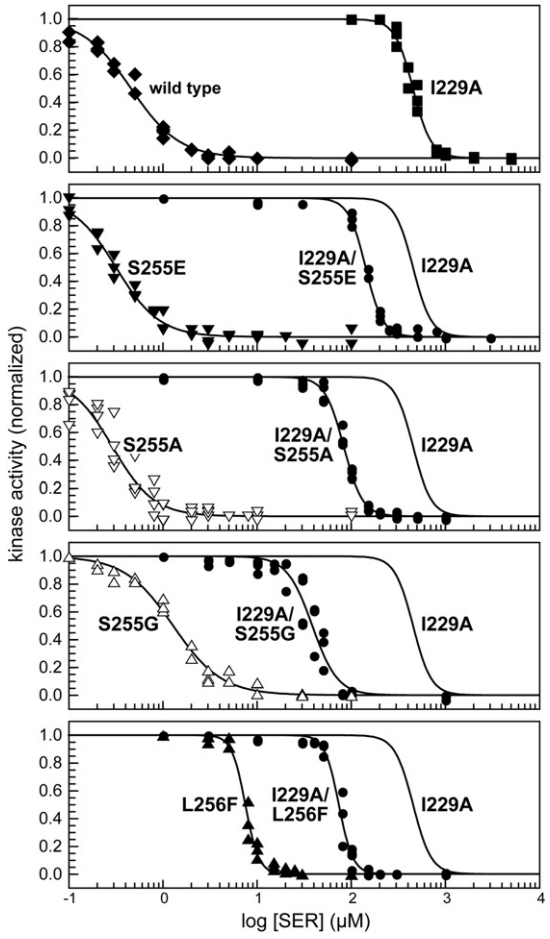

Fig. 5. Signaling properties of Tsr-HAMP mutants in an adaptation-proficient host. Panels show serine dose–response behaviors of UU2700 (CheR$^+$ CheB$^+$) cells expressing plasmid pPA114-encoded mutant receptors. Data from one or more independent *in vivo* FRET kinase experiments for each mutant receptor (see Materials and Methods) were jointly fitted to a Hill equation to illustrate the reproducibility of the measurements. Individual Hill fits for each experiment were averaged to obtain mean ± standard error values for $K_{1/2}$ (Table S1) and Hill coefficient (Table S2). The top panel shows data points for wild-type Tsr (black diamonds) and for Tsr-I229A (black squares). The four panels below show data points and dose–response curves for each suppressor alone and in combination with I229A. The response curve of Tsr-I229A (no data points) is included to illustrate the magnitude of the suppression effect on response threshold.

Modification of mutant receptors by the sensory adaptation enzymes

Adaptational modifications of receptors produce subunit mobility shifts in denaturing polyacrylamide gel electrophoresis (SDS-PAGE). Although the underlying mechanism is not well understood, each Q or methylated E (Em) residue at an adaptation site produces an incremental increase in electrophoretic mobility. Accordingly, we expressed mutant receptors in receptor-less host strains UU2610 (CheR$^-$ CheB$^-$), UU2611 (CheR$^-$ CheB$^+$), UU2632 (CheR$^+$ CheB$^-$), and UU2612 (CheR$^+$ CheB$^+$) and examined their SDS-PAGE band profiles to assess their propensities for adaptational modifications. All mutant receptors underwent modification by CheR and by CheB (Fig. S4). Tsr wild type, Tsr-S255A, and Tsr-S255E molecules were fully deamidated in the CheR$^-$ CheB$^+$ host and extensively methylated in the CheR$^+$ CheB$^-$ strain (Fig. 6 and Fig. S4). The on-biased suppressors exhibited similar patterns but were methylated less extensively (Tsr-S255G) or much less extensively (Tsr-L256F) than wild-type Tsr molecules in CheR$^+$ hosts, either before or after a serine stimulus (Fig. 6). Mutant receptors with I229A or I229S lesions, either alone or in combination with a suppressor, showed no fully modified molecules in the CheR$^+$ CheB$^-$ host (Fig. 6 and Fig. S4). In the CheR$^+$ CheB$^+$ host, a large serine stimulus (10 mM) elicited little, if any, increase in their modification state (Fig. 6 and Fig. S4).

Sensory adaptation behaviors of the mutant receptors

Sensory adaptation makes two vital contributions to the chemotactic behavior of *E. coli*. First, the modification states of the receptor molecules record the cell's recent chemical past, providing a short-term memory for sensing chemoeffector

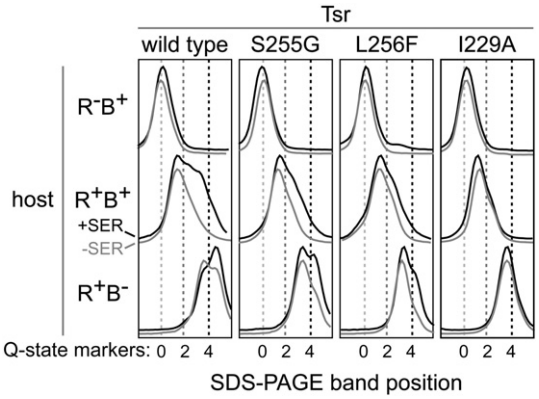

Fig. 6. Modification patterns of Tsr-HAMP mutant receptors in cells with different combinations of the CheR and CheB sensory adaptation enzymes. Plasmids encoding wild type or mutant Tsr were expressed in host strains UU2612 ($CheR^+$ $CheB^+$), UU2611 ($CheR^-$ $CheB^+$), and UU2632 ($CheR^+$ $CheB^-$). Tsr proteins were analyzed by SDS-PAGE and visualized by immunoblotting (see Materials and Methods). The positions of experimental gel bands (gray traces, no serine treatment; black traces, serine treated) and wild-type Tsr modification state markers (vertical broken lines; 0-Q = EEEEE, light gray; 2-Q = QEQEE, gray; 4-Q = QQQQE, black) were determined by densitometry. Traces were adjusted to the same maximum peak heights but offset vertically to facilitate comparisons between the −SER and +SER profiles in each host. The band position of each Tsr variant in the 2-Q (QEQEE) state (made in the $CheR^-$ $CheB^-$ host, UU2610) was very similar to or identical with that of the corresponding wild-type Tsr form (see Fig. S4).

concentration changes. Second, by tuning a receptor's detection threshold to match ambient chemoeffector levels, adaptation greatly extends the dynamic range for gradient sensing. Paradoxically, the doubly mutant receptors (I229A/S+ suppressor) produced robust chemotactic behaviors in tryptone semi-solid medium (Fig. 2) even though compromised in stimulus-induced methylation changes (Fig. S4). To assess their adaptation properties in more detail, we subjected mutant receptors in the FRET reporter strain UU2700 ($CheR^+$ $CheB^+$) to serine stimuli at their respective $K_{1/2}$ concentrations and followed their kinase activities over time (Fig. 7).

The off-biased receptors Tsr-S255E and Tsr-S255A exhibited wild-type adaptation behavior (Fig. 7): serine stimuli elicited a fast drop in kinase activity, followed by a slower return to the pre-stimulus activity level. During the recovery phase, the receptors evidently underwent a net increase in methylation state because, after adaptation was completed, serine removal caused a transient spike in kinase activity, reflecting the now excessive receptor methylation levels. These spike responses quickly returned to baseline activity as the sensory adaptation system reduced receptor methylation levels to the pre-stimulus modification state.

The two on-biased receptors Tsr-S255G and Tsr-L256F rapidly down-regulated kinase activity in response to serine stimuli but failed to fully adapt (Fig. 7). They quickly regained some kinase activity but recovery ceased well below the pre-stimulus kinase level. The S255G receptor showed a kinase spike upon serine removal, indicative of a net methylation increase during the adaptation phase

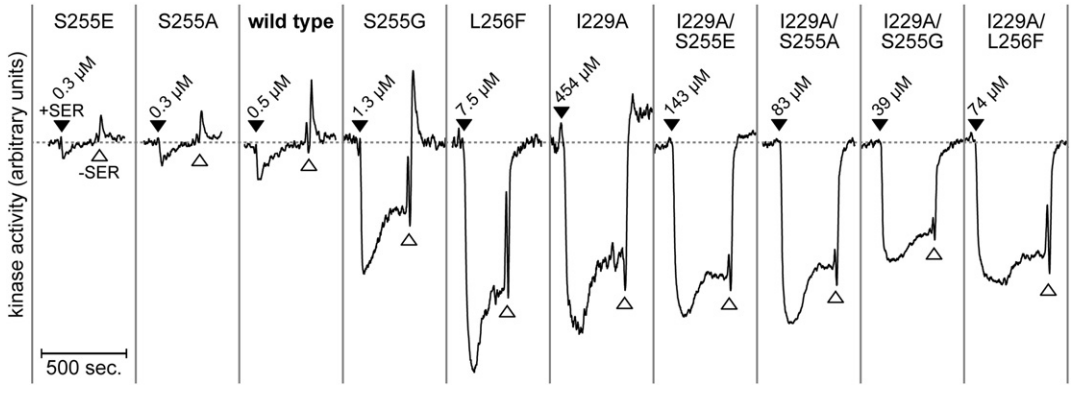

Fig. 7. Sensory adaptation properties of Tsr-HAMP mutant receptors. Cells of strain UU2700 ($CheR^+$ $CheB^+$) carrying pPA114-encoded mutant receptors were subjected to a serine stimulus (black triangles) at the $K_{1/2}$ concentration previously determined for each receptor. The ensuing FRET response was followed until kinase activity had stopped changing, at which time the serine was removed (white triangles). Note that the transient signal spike at the onset of serine removal is caused by a brief pause in solution flow, during which the cells consume some of the serine in the flow chamber. All traces are shown at the same time scale and the same relative activity scale, with pre-stimulus activity levels aligned. The magnitudes of the initial serine responses for each mutant receptor were scaled to reflect their relative kinase activity in strain UU2700 (Table S3).

(Fig. 7). Although the L256F receptor did not show a similar spike, we know that serine can elicit methylation increases in Tsr-L256F (Fig. 6). Most likely, the pre-stimulus kinase activity of L256F is essentially at the maximum possible level and cannot be further elevated by a methylation increase (Fig. 7 and Table S3). Tsr-I229A and its suppressor variants, which underwent no discernable serine-induced methylation increase (Fig. 6), showed partial adaptation responses and little, if any, kinase spike, both indicators of an adaptation defect (Fig. 7).

Discussion

Signaling behaviors of Tsr-HAMP mutants

The Tsr-HAMP domain controls signal output through its structural interactions with the adjoining MH bundle, which in turn modulates the conformation or dynamic motions of the receptor hairpin tip, where CheW and CheA bind (see Fig. 1a). The modification state of the four-helix MH bundle tunes the stimulus-responsive range of the receptor molecule: E residues at modification sites promote kinase-off output and enhance detection sensitivity, and Q and methylated E residues promote kinase-on output and reduce serine sensitivity. In this study, we used mutationally imposed modification states and cells with various combinations of the sensory adaptation enzymes, CheR and CheB, to characterize the signaling properties of Tsr mutants with amino acid replacements in packing layer 3 of the HAMP bundle. We describe receptor signaling behaviors in terms of equilibrium shifts between kinase-active and kinase-inactive output states: the S255E and S255A receptors exhibited shifts toward the OFF state, whereas the S255G and L256F suppressors were on-shifted (Fig. 8a). The I229A and I229S receptors, even in combination with a suppressor, were effectively locked in a kinase-on state except in cells containing both sensory adaptation enzymes (Fig. 8a).

Sensory adaptation effects on Tsr-HAMP signaling

In a CheR$^-$ CheB$^-$ host, only two of the mutant receptors (S255A and S255G) were serine responsive in the 2-Q modification state (Fig. 8a). In a CheR$^+$ CheB$^+$ host, all mutant receptors, including Tsr-I229A and Tsr-I229S, responded to serine (Fig. 8a). The sensory adaptation enzymes appear to augment receptor detection sensitivity in several ways. CheB most likely enhances sensitivity by driving receptor molecules to low modification states, thereby shifting them toward the kinase-off output state [19,29]. Consistent with this view, we found that the $K_{1/2}$ values for receptors in a CheR$^-$ CheB$^+$ host were very similar to those of their 5-E versions in a CheR$^-$ CheB$^-$ host (Table S4). Kim *et al.* have suggested that CheR also contributes to response sensitivity, possibly by binding to receptor molecules in the OFF state, the likely substrate for CheR-mediated methylation reactions [29]. Our

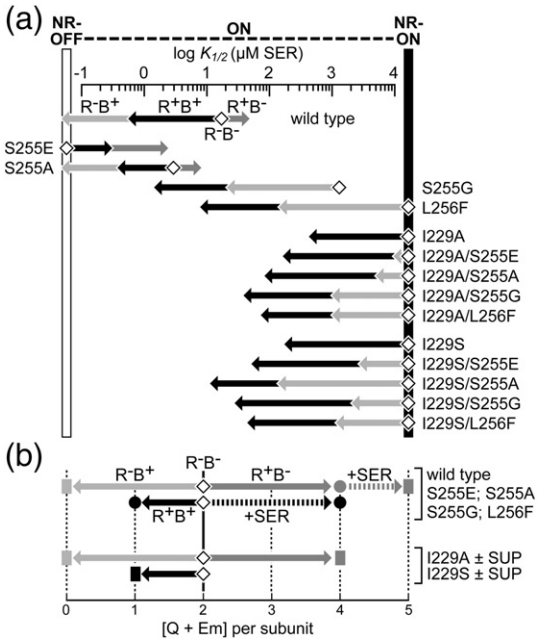

Fig. 8. Summary of Tsr-HAMP mutant receptor signaling properties. (a) Serine detection sensitivity in hosts with different combinations of CheR and CheB activities (data summarized in Table S4). White diamonds indicate response sensitivity in the 2-Q (QEQEE) state in a CheR$^-$ CheB$^-$ host (UU2567). Arrowheads indicate response sensitivities of the same receptors in hosts with one or both adaptation enzymes: CheR$^-$ CheB$^+$ (UU2699; light gray arrows); CheR$^+$ CheB$^-$ (UU2697; dark gray arrows); CheR$^+$ CheB$^+$ (UU2700; black arrows). NR-OFF denotes no response, no CheA kinase activity; NR-ON denotes no response, high CheA kinase activity. (b) Modification patterns in host strains with one or both adaptation enzymes. This summary is based on analyses of the gels shown in Fig. S4 and on comparisons of the mobilities of methylated species relative to their Q-state counterparts (data not shown). Continuous arrows indicate the majority subunit modification state before application of a saturating serine stimulus. The grayscale shading conventions for the four host strains corresponds to those used for the host strains in part (a) above. Broken arrows show modification states following a serine stimulus. Filled circles represent intermediate modification states that undergo further modification in response to serine; filled rectangles indicate end-point modification states (upper patterns) or ones that undergo no discernable serine response (lower patterns).

results provide evidence of such an effect: all on-shifted receptors were at least 10-fold more sensitive in a CheR$^+$ CheB$^+$ host than they were in a CheR$^-$ CheB$^+$ host (Table S4; Fig. 8a, black arrows) or in any uniform modification state in a host lacking both adaptation enzymes (Table S1; Fig. 8a, white diamonds). The threshold-lowering action of CheR was not evident in cells lacking CheB. For example, in a CheR$^+$ CheB$^-$ host, wild-type Tsr and the off-biased S255E and S255A receptors were shifted, presumably through CheR-mediated methylation, toward the ON state and reduced detection sensitivity (Fig. 8a, dark gray arrows). It may be that the CheR effect only operates on receptors that retain kinase-on output at low modification states.

Adaptational modifications of mutant receptors

All mutant receptors exhibited similar modification patterns in the absence of an overt serine stimulus (Fig. 8b): full deamidation in a CheR$^-$ CheB$^+$ host (Fig. 8b, light gray arrows), elevated methylation in a CheR$^+$ CheB$^-$ host (Fig. 8b, dark gray arrows), and net loss of one modification in a host with both enzymes (Fig. 8b, black arrows). Following a serine stimulus, wild-type Tsr and the four suppressor mutants underwent additional modification by CheR, whereas receptors with an I229 lesion did not (Fig. 8b, broken arrows). A majority of the serine-responsive receptors became fully modified, when CheR action was unopposed by CheB, and acquired 1–2 additional modifications in the host with both enzymes. In contrast, all receptors carrying I229A or I229S, even those in combination with a suppressor, failed to undergo detectable modification changes in response to serine stimuli (Fig. 8b, dark gray and black bars).

Serine did not elicit a behavioral response from I229 mutant receptors in a CheR$^+$ CheB$^-$ host (Fig. 8a), which could account for their lack of a serine-induced modification change in such a host (Fig. 8b). However, serine did elicit signaling responses from all I229 mutant receptors in a CheR$^+$ CheB$^+$ host (Fig. 8a) yet caused no discernable net change in their modification state (Fig. 8b). Assuming that CheR preferentially acts on receptors in the OFF state, whereas CheB preferentially operates on receptors in the ON state, the seemingly paradoxical behavior of I229 mutant receptors might reflect a lack of fine control over modification-induced signal state transitions. A saturating serine stimulus that drives the receptor population to the OFF state could trigger CheR action, but a single additional methylation might fully shift the mutant receptor molecule to the ON state, making it an excellent substrate for CheB action. Thus, serine stimuli might elicit futile cycles of CheR/CheB action on the mutant receptors, with little or no net change in their modification state.

Functional basis for suppression of Tsr-HAMP signaling defects

In a CheR$^+$ CheB$^+$ host, all suppressor-containing receptors mediate chemotactic responses on semi-solid tryptone agar; Tsr-I229A and Tsr-I229S do not. Chemotactic performance on tryptone reflected the serine detection sensitivities of the receptors. Although in adaptation-proficient cells, the I229A and I229S receptors responded to serine step changes in FRET experiments, their $K_{1/2}$ values (454 and 254 μM, respectively) were only slightly below the serine concentration in tryptone (~670 μM). The suppressors lowered I229A and I229S response thresholds to the range 10–150 μM, evidently sufficient for detection of metabolism-generated serine gradients in tryptone medium. However, the doubly mutant receptors could not mediate chemotaxis on semi-solid agar containing 100 μM serine, whereas receptors with lower serine thresholds could. As a general rule, it appears that a receptor's $K_{1/2}$ value must be at least 10-fold below the medium serine concentration to mount a chemotactic response (Table S4). For example, the wild-type, S255E, and S255A receptors ($K_{1/2} \leq 0.5$ μM) produced chemotactic responses at 4 μM or higher serine; S255G ($K_{1/2} = 1.3$ μM) promoted chemotaxis at 20 μM or higher serine; and L256F ($K_{1/2} = 7.5$ μM) promoted chemotaxis at 100 μM or higher serine.

The suppressor derivatives of I229A and I229S showed incomplete adaptation to a $K_{1/2}$ serine stimulus in the CheR$^+$ CheB$^+$ host (Fig. 7) and underwent no discernable change in modification state in response to a large serine increase (Fig. 8b). These flawed sensory adaptation behaviors evidently do not prevent colony expansion in semi-solid media, a behavior universally interpreted as chemotaxis. Whether partial adaptation occurs through a methylation-independent mechanism, for example, stimulus-induced reorganization of receptor signaling teams or networking connections in the receptor array [30,31], remains an open question.

Mechanistic basis for suppression of Tsr-HAMP signaling defects

Although there are no high-resolution structures for HAMP domains in orthodox MCP family chemoreceptors, several lines of evidence indicate that they have a parallel four-helix bundle architecture similar to that of the Af1503 and Aer2 HAMP domains [3]. In Tsr, the HAMP residues most critical to function correspond to the hydrophobic residues that promote packing interactions between the HAMP helices [14,15]. Accordingly, Tsr-HAMP residue I229, by analogy to A291 of Af1503-HAMP [8], most likely projects into the hydrophobic core of the four-helix bundle and makes an important contribution to its packing stability (see Fig. 1b). An alanine or serine replacement at I229 effectively locks Tsr in a kinase-on mode. Amino acid replacements at S255

or L256 in the same HAMP packing layer suppress those signaling defects by shifting output toward the OFF signaling state, thereby enhancing serine sensitivity. Amino acid replacements outside of packing layer 3 cannot suppress the signaling defects of amino acid replacements at residue 229 [15], suggesting that only local changes in the structure or packing stability of HAMP layer 3 are able to restore serine responsiveness in the I229A and I229S mutant receptors. Below, we consider these suppression effects in the context of two different HAMP signaling models.

A two-conformation model of HAMP signaling

The gearbox model proposes that the ON and OFF output states of the receptor correspond to alternative helix-packing arrangements of the HAMP bundle (Fig. 9) [8]. In the complementary *x-da* arrangement, three residues contribute to packing interactions in each bundle layer. Tsr-HAMP residue 229 would occupy the central *x* position in this conformation, whereas residues 255 and 256 would play equivalent packing roles in flanking positions (Fig. 9). In the *a-d* arrangement, residues 229 and 256 would play equivalent packing roles; residue 255 would be peripheral to the hydrophobic core (Fig. 9). This model posits that the side-chain volume of the *x* residue in HAMP layer 3 is a principal determinant of overall bundle configuration. Small side chains should favor *x-da* packing; large side chains should favor *a-d* packing. Because Tsr-I229A and Tsr-I229S have extremely on-biased outputs, it follows that the *x-da* configuration should correspond to the ON state and the *a-d* conformation should represent the OFF state. These state assignments are consonant with structural and signaling studies of Af1503-HAMP variants in chimeric signaling proteins [11,32].

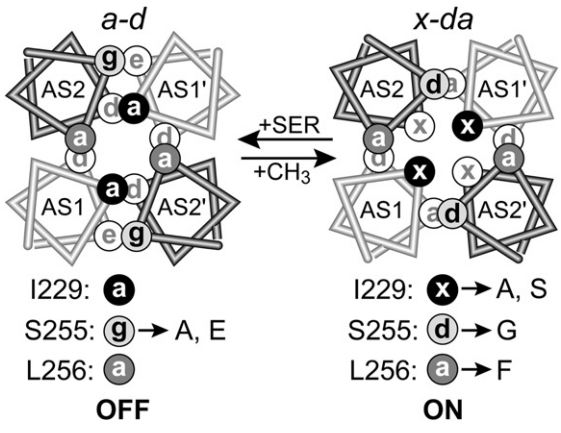

Fig. 9. A two-conformation model of HAMP signaling. Helical wheel diagrams (viewed in the N-to-C direction) of alternative packing arrangements of HAMP helices proposed by the gearbox model [8]. The shaded circles indicate Tsr residues in packing layer 3: I229 (black), S255 (light gray), and L256 (dark gray); see Fig. 1b. Residues indicated by white circles and gray labels are in packing layer 4. In the *a-d* arrangement, I229 and L256 occupy typically hydrophobic *a* positions; S255 occupies a peripheral *g* position. In the *x-da* arrangement, I229 has a central *x* position at the bundle core; S255 and L256 occupy flanking *d* and *a* packing positions, respectively. Based on published mutant HAMP structures [8,11], signaling properties [11], and the signaling properties of the Tsr mutants described in this study, the gearbox model predicts that *a-d* packing corresponds to the OFF state, whereas *x-da* packing corresponds to the ON state.

Strictly interpreted, the gearbox model must explain the signaling properties of HAMP mutant receptors in terms of equilibrium shifts between the native *a-d* and *x-da* signaling conformations. Off-biased lesions (S255E and; S255A) should favor the *a-d* packing arrangement; on-biased lesions (S255G, L256F, I229A, and I229S) should shift HAMP toward the *x-da* state (Fig. 9). These changes must alter the relative structural stabilities of the two HAMP signaling conformations. Accordingly, off-biased changes (S255E and S255A) could suppress the locked-on defects of the I229A and I229S receptors by reducing the free-energy difference between the two signaling states. However, it is difficult to extend this analysis to the on-biased suppressors, which would be expected to exacerbate the free-energy difference between the ON and OFF states in doubly mutant receptors.

A conformational ensemble model of HAMP signaling

The dynamic-bundle model of HAMP signaling arose from extensive genetic studies of Tsr-HAMP missense and deletion mutants [3,14–17]. It proposes that the Tsr-HAMP bundle, when connected to adjoining input and output structural elements, operates over a range of related conformations that differ in the stability of the AS2/AS2′ helix-packing interactions (Fig. 10a). The *a-d* and *x-da* packing arrangements proposed by the gearbox model might represent two of those conformational states. However, the dynamic-bundle model addresses general aspects of HAMP packing stability because there is as yet no direct, high-resolution structural information for the Tsr-HAMP bundle. The AS2/AS2′ helices connect to the MH1/MH1′ helices of the methylation bundle through a four-residue phase stutter that is proposed to couple the HAMP and MH bundles in structural opposition (Fig. 10a): loosely packed MH bundles produce kinase-off output, and more stably packed MH bundles produce kinase-on output. Although both the ON and OFF signaling states might correspond to multiple HAMP structures, the evidence for conformational ensembles is more compelling for

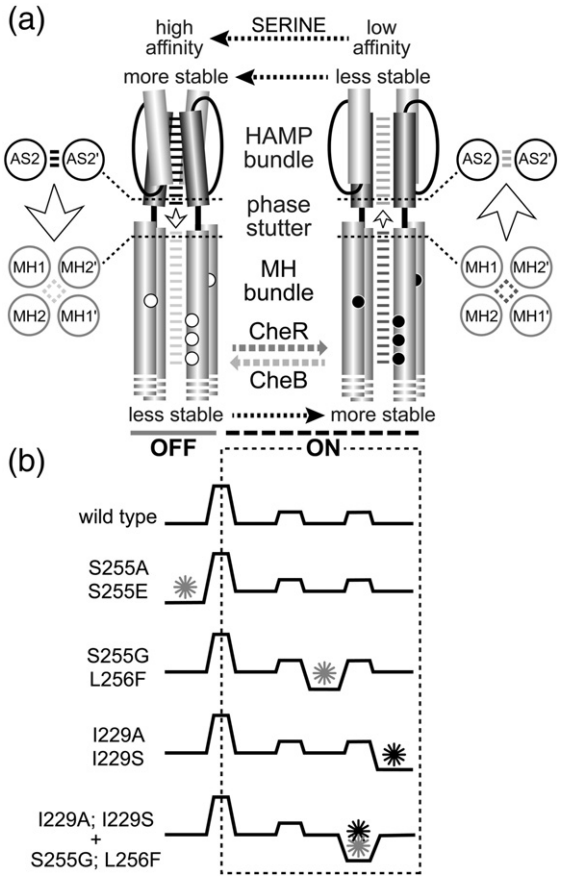

Fig. 10. A conformational ensemble model of HAMP signaling. (a) Packing stabilities and structural interactions of the HAMP and MH bundles predicted by the dynamic-bundle model [15]. An intervening phase stutter connection between the AS2/AS2′ and MH1/MH1′ helices couples the two bundle structures in opposition such that enhanced packing stability of one reduces packing stability of the other. Attractant inputs promote HAMP stability; high modification states promote MH bundle stability. The model further proposes that CheR operates most efficiently on loosely packed methylation helices, whereas CheB acts most efficiently on more stably packed MH bundles. The OFF state could be a discrete species, but the Tsr system has multiple ON states with different serine affinities and CheR/CheB substrate properties [3,16,17,41]. (b) Energy landscape diagrams of the HAMP bundle in various mutant receptors. In this simplified example, one HAMP conformation produces kinase-off output; three isoenergetic conformations produce kinase-on output (regime inside broken outline). In actuality, Tsr-HAMP might operate over a more continuous range of conformational and dynamic states. Structural lesions (asterisks) that enhance the stability of one HAMP packing arrangement relative to the others shift receptors toward the OFF or ON output states, thereby altering their detection sensitivity. Gray asterisks indicate HAMP structural changes that suppress locked-on I229 lesions (black asterisk) in doubly mutant receptors. In this model, the on-biased suppressors (S255G and L256F) act by destabilizing the locked-on HAMP structure, shifting the bundle of the doubly mutant receptor to a kinase-on, but serine-responsive, conformational or dynamic state.

the ON state. First, many different amino acid replacements at key HAMP bundle-packing residues (e.g., I229A, S255G, L256F) shift output toward the ON state [16] as do deletions that ablate various HAMP structural elements (e.g., the AS2 helices) [17]. Thus, receptors with a variety of non-native HAMP bundles, or lacking HAMP altogether, can produce kinase-on output. Second, the MH bundles in different on-biased HAMP mutants respond differently to the sensory adaptation enzymes and to adaptational modifications. For example, Tsr-S255G has near-normal modification patterns, Tsr-I229A has altered modification behaviors, and TsrΔHAMP is not a substrate for any adaptational modifications. However, all three mutant receptors produce kinase-on output. These functional differences imply that on-shifted HAMP domains can have different conformations or dynamic behaviors.

According to the dynamic-bundle model, HAMP domains have dynamic conformational states, a number of which produce kinase-on output. A HAMP energy landscape with several ON states illustrates how on-shifted HAMP lesions (S255G and L256F) might suppress the signaling defects caused by locked-on HAMP lesions (I229A and I229S) (Fig. 10b). We suggest that the S255G and L256F suppressors and the I229A and I229S lesions favor different kinase-on HAMP conformations. Thus, in doubly mutant receptors, the on-biased suppressors could serve to destabilize the locked-on conformation caused by the I229 lesion, resulting in a more serine-responsive kinase-on HAMP bundle conformation.

Are HAMP domains dynamic signaling devices?

The behaviors of the mutant receptors in this report seem most easily explained by a HAMP signaling model that allows for multiple ON conformations, perhaps distinguished by their dynamic properties. Conformational ensemble models can account for alleviation of locked-on defects by on-biased suppressors by proposing that the interacting HAMP alterations individually favor different ON conformations. A discrete, two-conformation signaling model can only account for such suppression effects through compensatory structural interactions of the HAMP lesions. For example, the L256F change might favor the *x-da* (ON) conformation when a bulky wild-type isoleucine is its neighbor at residue 229, but it might better accommodate *a-d* packing with a smaller A or S residue at position 229 (Fig. 9). Similarly, S255G could conceivably favor the OFF state when paired with I229A or I229S, although a plausible structural basis for that interaction is less apparent. Additional structural studies of mutant HAMP domains, preferably with their adjoining structural elements, could cast valuable light on these mechanistic issues.

Materials and Methods

Bacterial strains

All strains were derivatives of *E. coli* K12 strain RP437 [33]. Their relevant genotypes are as follows: UU2610 [Δ*aer*-1 Δ(*tar-cheB*)4346 Δ*tsr*-5547 Δ*trg*-4543] [16]; UU2611 [Δ*aer*-1 Δ(*tar-cheR*)4283 Δ*tsr*-5547 Δ*trg*-4543] [16]; UU2612 [Δ*aer*-1 Δ(*tar-tap*)4530 Δ*tsr*-5547 Δ*trg*-4543] [16]; UU2632 [Δ*aer*-1 Δ(*tar-tap*)4530 Δ*cheB*-4345 Δ*tsr*-5547 Δ*trg*-4543] [16]; UU2567 [Δ(*tar-cheZ*)4211 Δ*tsr*-5547 Δ*trg*-4543 Δ*aer*-1] (this work); UU2697 [Δ(*cheY-cheZ*)1215 Δ*aer*-1 Δ(*tar-tap*)4530 Δ*cheB*-4345 Δ*tsr*-5547 Δ*trg*-4543] (this work); UU2699 [Δ(*cheY-cheZ*)1215 Δ*aer*-1 Δ(*tar-cheR*)4283 Δ*tsr*-5547 Δ*trg*-4543] (this work); UU2700 [Δ(*cheY-cheZ*)1215 Δ*aer*-1 Δ(*tar-tap*)4530 Δ*tsr*-5547 Δ*trg*-4543] (this work).

Plasmids

Plasmids used in this study were as follows: pKG116, a derivative of pACYC184 [34] that confers chloramphenicol resistance and has a sodium salicylate inducible *nahR* promoter [35]; pPA114, a relative of pKG116 that carries wild-type *tsr* under *nahR* promoter control [36]; and pVS88, a derivative of pTrc99A that carries *cheY-YFP* and *cheZ-CFP* under IPTG-inducible control [23].

Chemotaxis assays on semi-solid agar media

Strain UU2612 hosting Tsr expression plasmids was assessed for chemotactic ability on tryptone or minimal serine semi-solid agar plates containing 12.5 μg/ml chloramphenicol and 0.6 μM sodium salicylate as previously described [37]. Tryptone plates were incubated at 30 °C or 32.5 °C for 6–8 h; minimal plates were incubated at 30 °C for 15 h.

Site-directed mutagenesis

Mutations in the *tsr* coding region of plasmid pPA114 were generated by QuikChange PCR mutagenesis as previously described [36]. All mutational changes were verified by sequencing the entire *tsr* coding region in the mutant plasmid.

Assessing receptor modification patterns

Tsr molecules with different adaptational modifications states were resolved by SDS-PAGE and visualized by immunoblotting as previously described [38]. Various host strains carrying Tsr expression plasmids were assayed in the presence and absence of 10 mM L-serine as previously described [39]. Tsr band intensities were quantified by densitometry, using NIH ImageJ software[†], and subsequent data analysis and plotting with KaleidaGraph 4.1 software (Synergy Software).

FRET-based measurement of *in vivo* kinase activity

FRET instrumentation, experimental protocol, and data analysis were essentially as described by Sourjik *et al.* [23].

Preparation of cells

For all experiments, host cells carried a pPA114 derivative expressing a Tsr variant and plasmid pVS88, expressing the CheZ-CFP (donor) and CheY-YFP (acceptor) FRET reporter pair. Overnight starter cultures were prepared by growing cells to saturation at 30 °C in tryptone broth with antibiotics (50 μg/ml ampicillin and 12.5 μg/ml chloramphenicol) but no inducers. For experiments, fresh overnight cultures were diluted 100-fold into 10 ml tryptone broth containing antibiotics (50 μg/ml ampicillin and 12.5 μg/ml chloramphenicol) and expression inducers (50 μM IPTG and 0.6 μM sodium salicylate). Cultures were grown in shaking incubators at 30 °C to an optical density (at 600 nm) of 0.5 before harvesting in a tabletop centrifuge at ~1000*g* for 6 min. Cells were washed twice with 5 ml motility buffer [10 mM potassium phosphate buffer (pH 7.0), 100 μM K ethylenediaminetetraacetic acid, 10 mM Na lactate, and 100 μM L-methionine] and resuspended in 10 ml of motility buffer. Washed cells were maintained at 4 °C for at least 30 min before use.

Adding cells to polylysine-coated coverslips

Round glass coverslips (12 mm diameter, #1 thickness, and FisherBrand) were coated with poly-L-lysine in advance of FRET experiments. Coverslips were cleaned by washing with double-distilled water, then 70% ethanol, then double-distilled water, and then air dried. We placed 20 μl of 0.1% (w/v) poly-L-lysine solution (Sigma) at the center of a coverslip, allowed it to stand for about 30 min, and then removed it by aspiration. Coverslips were then washed three times with 100 μl double-distilled water and air dried. Cell samples (see above) were added by pelleting 1.5 ml of processed cells by centrifugation at ~6000*g* for 2 min. The cell pellet was resuspended in 50 μl motility buffer and 50 μl of the concentrated cell suspension was placed at the center of a polylysine-coated coverslip and allowed to stand at room temperature for about 10 min.

Assembling the flow cell

Coverslips with cells attached were placed face-down in the upper opening of a flow cell, fabricated to the specifications of Berg and Block [40] except that the center hole, square in the original design, was changed to a circular opening with the same diameter to accommodate round coverslips. The lower opening of the flow cell was sized for a round 25-mm, #1 coverslip (VWR). Both the top and bottom coverslips were sealed to the flow chamber with a continuous bead of Apiezon H grease around their edges. A syringe pump was used to draw solutions through the flow chamber at a constant rate. All experiments in the present study used a flow rate of 1000 μl/min. We tested the modified flow cell by measuring liquid displacement rates at five different locations in the circular opening (center and near the outer edge at 45°, 125°, 225°, and 315°) by switching from water to fluorescein solution and found that solution flow was uniform throughout.

FRET instrumentation

Flow cells were housed in an aluminum chamber whose temperature was controlled by a circulating water bath. All

experiments in this study were performed at 30 °C. The sample chamber was mounted on the stage of a Zeiss Axio Observer inverted microscope. Fields of 300–500 cells were observed with a PlanFluor 40× objective. The cell sample was excited by a 75-W xenon source (Zeiss XBO 75), attenuated 1000-fold by a neutral density filter, and transmitted through an excitation bandpass filter (Semrock FF01-438/24-25) and a dichroic mirror (Semrock FF458-Di02-25X36). The epifluorescent emission from the cells was split by a second dichroic mirror (Chroma 515DCXR) into "<515 nm" and ">515 nm" wavelength channels, which were measured by photon-counting photomultipliers (Hamamatsu H7421-40) after passing through CFP and YFP emission bandpass filters (Semrock FF01-483/32-25 and FF01-542/27-25), respectively. The photon counts from each channel were acquired by a data acquisition board (National Instrument PCIe-6251) and recorded in 1-s bins by a computer via LabView program (National Instrument).

FRET data analysis

Theory

The ratio of YFP to CFP signals (R) provides a robust measure of FRET activity, which in turn reflects receptor-dependent CheA kinase activity [23]. Attractant stimuli that reduce CheA activity decrease the YFP signal and increase the CFP signal. The absolute ratio (α) of those signal changes reflects the efficiency of energy transfer between the two fluorescent proteins and is constant for a given instrument. In our system setup, α = 1.08. Thus,

$$A_S = (R_B - R_0 - R_S)/(\alpha + R_0 + \Delta R_S)$$

where A_S is the amount of residual kinase activity after application of an attractant, R_B is the YFP/CFP ratio before the stimulus, R_0 is the YFP/CFP ratio in the absence of FRET, and ΔR_S is the change in YFP/CFP ratio in response to the stimulus [23,26]. We define the maximum amount of receptor-regulated kinase activity (A_{max}) as the FRET change elicited by a saturating stimulus, that is, from the largest value of ΔR_S in a stimulus series:

$$A_{max} = (R_B - R_0)/(\alpha + R_B)$$

Practice

FRET data were processed, fitted, and plotted in KaleidaGraph 4.1 (Synergy Software). To reduce signal noise, we smoothed raw photon counts from the YFP and CFP channels with a running average calculation in a 10-s window before further analysis. We calculated A_S values for all stimulus applications in an experiment and then normalized them to the A_{max} value in that experiment. The dose–response data for relative kinase activities as a function of attractant concentration were fitted to a multisite Hill equation:

$$A_S/A_{max}([L]) = 1 - \left([L]^H / \left([L]^H + K_{1/2}^H\right)\right)$$

where [L] is the concentration of the attractant ligand, $K_{1/2}$ is the attractant concentration that inhibits 50% of the kinase activity, and H is the Hill coefficient [23].

Protein structural display

Structure images were prepared with PyMOL (Mac) software‡.

Acknowledgements

We thank Peter Ames (University of Utah) for providing the dose–response data for wild-type Tsr in different modification states (Fig. 3) and Ady Vaknin (Hebrew University) for suggesting the KCN assay for kinase activity and for other helpful discussions. Peter Ames, Ady Vaknin, Joachim Schultz (University of Tübingen), Victor Sourjik (University of Heidelberg), and Claudia Studdert (National University, Mar del Plata) kindly provided editorial and scientific comments on the manuscript. Special thanks go to Victor Sourjik for much valuable advice and material support that enabled us to set up the FRET-based kinase assay. This work was supported by National Institutes of Health research grant GM19559 from the National Institute of General Medical Sciences and by a supplemental award issued under the American Recovery and Reinvestment Act of 2009. The Protein–DNA Core Facility at the University of Utah receives support from National Cancer Institute grant CA42014 to the Huntsman Cancer Institute.

Appendix A. Supplementary data

Supplementary data to this article can be found online at http://dx.doi.org/10.1016/j.jmb.2014.08.003.

Received 26 May 2014;
Received in revised form 7 July 2014;
Accepted 3 August 2014
Available online 15 August 2014

Keywords:
chemotaxis;
transmembrane signaling;
sensory adaptation

†http://rsb.info.gov/ij/.
‡http://www.pymol.org.

Abbreviations used:
FRET, Förster resonance energy transfer; MCP, methyl-accepting chemotaxis protein; MH, methylation helix.

References

[1] Alexander RP, Zhulin IB. Evolutionary genomics reveals conserved structural determinants of signaling and adaptation in microbial chemoreceptors. Proc Natl Acad Sci USA 2007;104:2885–90.

[2] Hazelbauer GL, Falke JJ, Parkinson JS. Bacterial chemoreceptors: high-performance signaling in networked arrays. Trends Biochem Sci 2008;33:9–19.

[3] Parkinson JS. Signaling mechanisms of HAMP domains in chemoreceptors and sensor kinases. Annu Rev Microbiol 2010;64:101–22.

[4] Kim KK, Yokota H, Kim SH. Four-helical-bundle structure of the cytoplasmic domain of a serine chemotaxis receptor. Nature 1999;400:787–92.

[5] Falke JJ, Hazelbauer GL. Transmembrane signaling in bacterial chemoreceptors. Trends Biochem Sci 2001;26: 257–65.

[6] Hazelbauer GL, Lai WC. Bacterial chemoreceptors: providing enhanced features to two-component signaling. Curr Opin Microbiol 2010;13:124–32.

[7] Dunin-Horkawicz S, Lupas AN. Comprehensive analysis of HAMP domains: implications for transmembrane signal transduction. J Mol Biol 2010;397:1156–74.

[8] Hulko M, Berndt F, Gruber M, Linder JU, Truffault V, Schultz A, et al. The HAMP domain structure implies helix rotation in transmembrane signaling. Cell 2006;126:929–40.

[9] Airola M, Watts KJ, Crane BR. Structure of concatenated HAMP domains provides a mechanism for signal transduction. Structure 2010;18:436–48.

[10] Airola MV, Sukomon N, Samanta D, Borbat PP, Freed JH, Watts KJ, et al. HAMP domain conformers that propagate opposite signals in bacterial chemoreceptors. PLoS Biol 2013;11:e1001479.

[11] Ferris HU, Dunin-Horkawicz S, Mondejar LG, Hulko M, Hantke K, Martin J, et al. The mechanisms of HAMP-mediated signaling in transmembrane receptors. Structure 2011;19:378–85.

[12] Swain KE, Falke JJ. Structure of the conserved HAMP domain in an intact, membrane-bound chemoreceptor: a disulfide mapping study. Biochemistry 2007;46:13684–95.

[13] Watts KJ, Johnson MS, Taylor BL. Structure-function relationships in the HAMP and proximal signaling domains of the aerotaxis receptor Aer. J Bacteriol 2008;190: 2118–27.

[14] Ames P, Zhou Q, Parkinson JS. Mutational analysis of the connector segment in the HAMP domain of Tsr, the *Escherichia coli* serine chemoreceptor. J Bacteriol 2008;190:6676–85.

[15] Zhou Q, Ames P, Parkinson JS. Mutational analyses of HAMP helices suggest a dynamic bundle model of input–output signalling in chemoreceptors. Mol Microbiol 2009;73:801–14.

[16] Zhou Q, Ames P, Parkinson JS. Biphasic control logic of HAMP domain signalling in the *Escherichia coli* serine chemoreceptor. Mol Microbiol 2011;80:596–611.

[17] Ames P, Zhou Q, Parkinson JS. HAMP domain structural determinants for signalling and sensory adaptation in Tsr, the *Escherichia coli* serine chemoreceptor. Mol Microbiol 2014; 91:875–86.

[18] Ferris HU, Zeth K, Hulko M, Dunin-Horkawicz S, Lupas AN. Axial helix rotation as a mechanism for signal regulation inferred from the crystallographic analysis of the *E. coli* serine chemoreceptor. J Struct Biol 2014;186:349–56.

[19] Sourjik V, Berg HC. Receptor sensitivity in bacterial chemotaxis. Proc Natl Acad Sci USA 2002;99:123–7.

[20] Klavon J. BD Bionutrients Technical Manual. Sparks, MD: BD Biosciences; 2006.

[21] Rice MS, Dahlquist FW. Sites of deamidation and methylation in Tsr, a bacterial chemotaxis sensory transducer. J Biol Chem 1991;266:9746–53.

[22] Han XS, Parkinson JS. An unorthodox sensory adaptation site in the *Escherichia coli* serine chemoreceptor. J Bacteriol 2014;196:641–9.

[23] Sourjik V, Vaknin A, Shimizu TS, Berg HC. *In vivo* measurement by FRET of pathway activity in bacterial chemotaxis. Methods Enzymol 2007;423:363–91.

[24] Taylor BL, Miller JB, Warrick HM, Koshland DE. Electron acceptor taxis and blue light effect on bacterial chemotaxis. J Bacteriol 1979;140:567–73.

[25] Endres RG, Oleksiuk O, Hansen CH, Meir Y, Sourjik V, Wingreen NS. Variable sizes of *Escherichia coli* chemoreceptor signaling teams. Mol Syst Biol 2008;4:211.

[26] Shimizu TS, Tu Y, Berg HC. A modular gradient-sensing network for chemotaxis in *Escherichia coli* revealed by responses to time-varying stimuli. Mol Syst Biol 2010;6:382.

[27] Bornhorst JA, Falke JJ. Evidence that both ligand binding and covalent adaptation drive a two-state equilibrium in the aspartate receptor signaling complex. J Gen Physiol 2001; 118:693–710.

[28] Li G, Weis RM. Covalent modification regulates ligand binding to receptor complexes in the chemosensory system of *Escherichia coli*. Cell 2000;100:357–65.

[29] Kim C, Jackson M, Lux R, Khan S. Determinants of chemotactic signal amplification in *Escherichia coli*. J Mol Biol 2001;307:119–35.

[30] Sourjik V, Armitage JP. Spatial organization in bacterial chemotaxis. EMBO J 2010;29:2724–33.

[31] Frank V, Vaknin A. Prolonged stimuli alter the bacterial chemosensory clusters. Mol Microbiol 2013;88:634–44.

[32] Mondejar LG, Lupas A, Schultz A, Schultz JE. HAMP domain-mediated signal transduction probed with a mycobacterial adenylyl cyclase as a reporter. J Biol Chem 2012; 287:1022–31.

[33] Parkinson JS, Houts SE. Isolation and behavior of *Escherichia coli* deletion mutants lacking chemotaxis functions. J Bacteriol 1982;151:106–13.

[34] Chang ACY, Cohen SN. Construction and characterization of amplifiable multicopy DNA cloning vehicles derived from the p15A cryptic miniplasmid. J Bacteriol 1978;134:1141–56.

[35] Buron-Barral M, Gosink KK, Parkinson JS. Loss- and gain-of-function mutations in the F1-HAMP region of the *Escherichia coli* aerotaxis transducer Aer. J Bacteriol 2006;188:3477–86.

[36] Ames P, Studdert CA, Reiser RH, Parkinson JS. Collaborative signaling by mixed chemoreceptor teams in *Escherichia coli*. Proc Natl Acad Sci USA 2002;99:7060–5.

[37] Parkinson JS. *cheA*, *cheB*, and *cheC* genes of *Escherichia coli* and their role in chemotaxis. J Bacteriol 1976;126:758–70.

[38] Mowery P, Ostler JB, Parkinson JS. Different signaling roles of two conserved residues in the cytoplasmic hairpin tip of Tsr, the *Escherichia coli* serine chemoreceptor. J Bacteriol 2008;190:8065–74.

[39] Slocum MK, Parkinson JS. Genetics of methyl-accepting chemotaxis proteins in *Escherichia coli*: null phenotypes of the *tar* and *tap* genes. J Bacteriol 1985;163:586–94.

[40] Berg HC, Block SM. A miniature flow cell designed for rapid exchange of media under high-power microscope objectives. J Gen Microbiol 1984;130:2915–20.

[41] Stewart V. The HAMP signal-conversion domain: static two-state or dynamic three-state? Mol Microbiol 2014;91:853–7.

Fig. S1 Chemotaxis phenotypes of Tsr-HAMP mutants on minimal semi-solid agar. Plates containing minimal salts medium supplemented with various serine concentrations and with 1 mM glycerol and 0.6 μM salicylate were inoculated with UU2612 cells carrying the indicated pPA114 mutant receptors. Plates were incubated at 30°C for 18 hours.

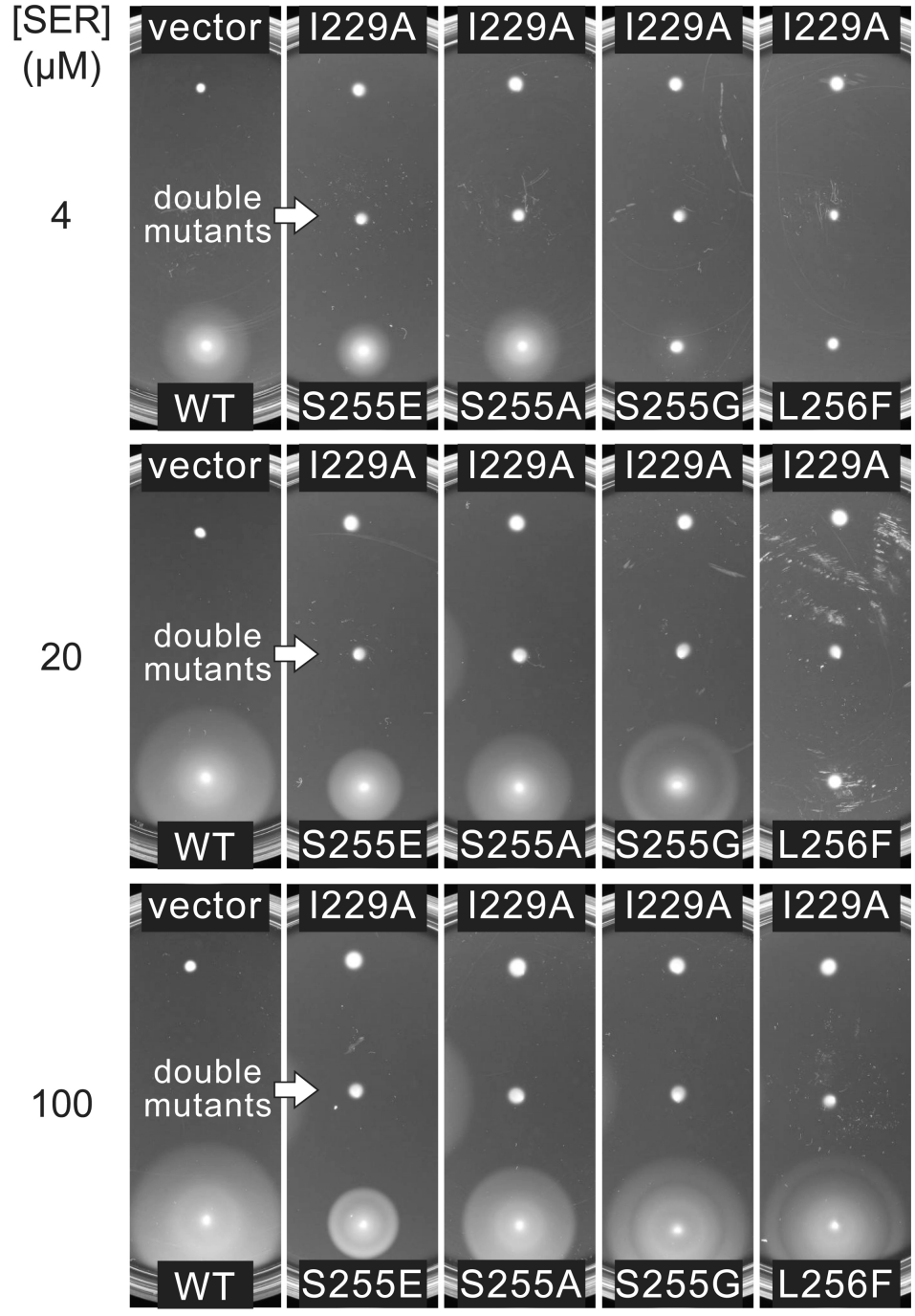

Fig. S2 Examples of kinase activity measurements in strain UU2567 (R^- B^-). Kinase activities of receptor signaling complexes can be calculated from the FRET (YFP/CFP ratio) change induced by a saturating (10 mM) serine stimulus (wild-type Tsr [QQQQE] and Tsr-L256F [EEEEE] or from the FRET change induced by 3 mM KCN treatment (wild-type Tsr [EEEEE] and Tsr-L256F [QQQQE]. Considered together, the serine and KCN responses identify receptors with lock-off (wild-type Tsr [EEEEE] and lock-on (Tsr-L256F [QQQQE] signaling activities.

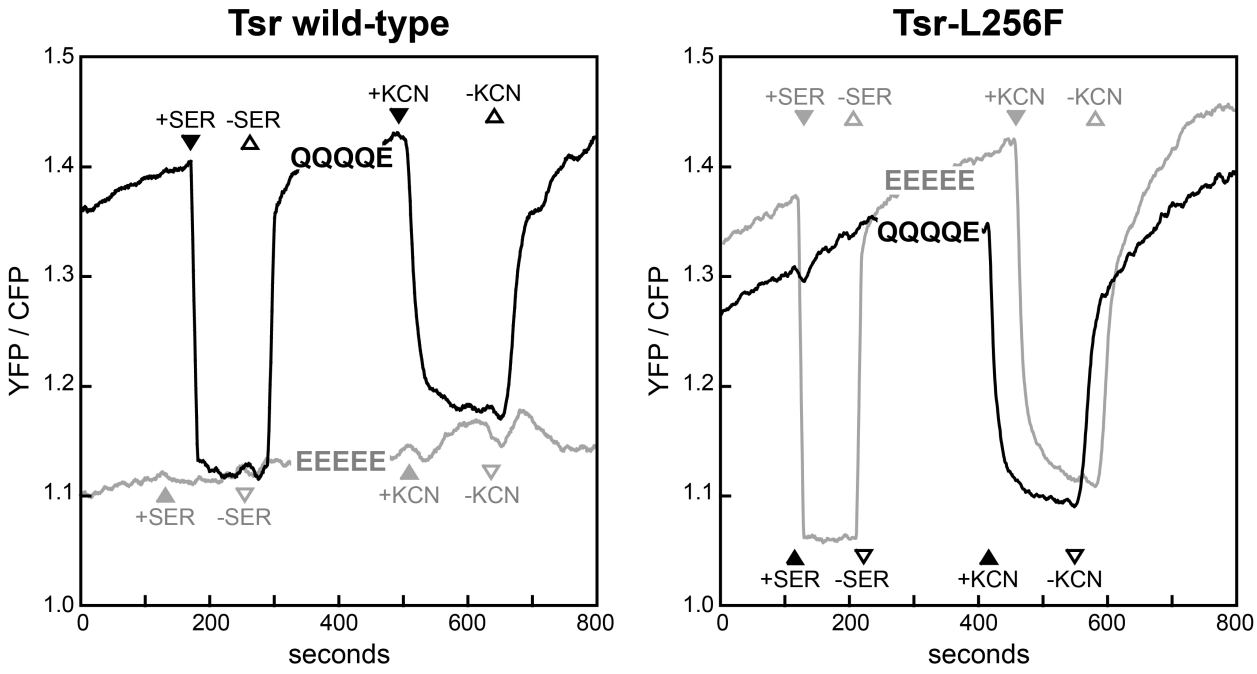

Fig. S3 Signaling properties of Tsr-I229S receptors in an adaptation-proficient host. Panels show serine dose-response behaviors of UU2700 ($CheR^+$ $CheB^+$) cells expressing plasmid pPA114-encoded mutant receptors. Data from one or more independent *in vivo* FRET kinase experiments for each mutant receptor (see Methods) were jointly fitted to a Hill equation to illustrate the reproducibility of the measurements. Individual Hill fits for each experiment were averaged to obtain mean ± standard error values for $K_{1/2}$ (Table S1) and Hill coefficient (Table S2). The top panel shows data points for wild-type Tsr (black diamonds) and for Tsr-I229S (black squares). The four panels below show data points and dose-response curves for each suppressor alone and in combination with I229S. The response curve of Tsr-I229S (no data points) is included to illustrate the magnitude of the suppression effect on response threshold .

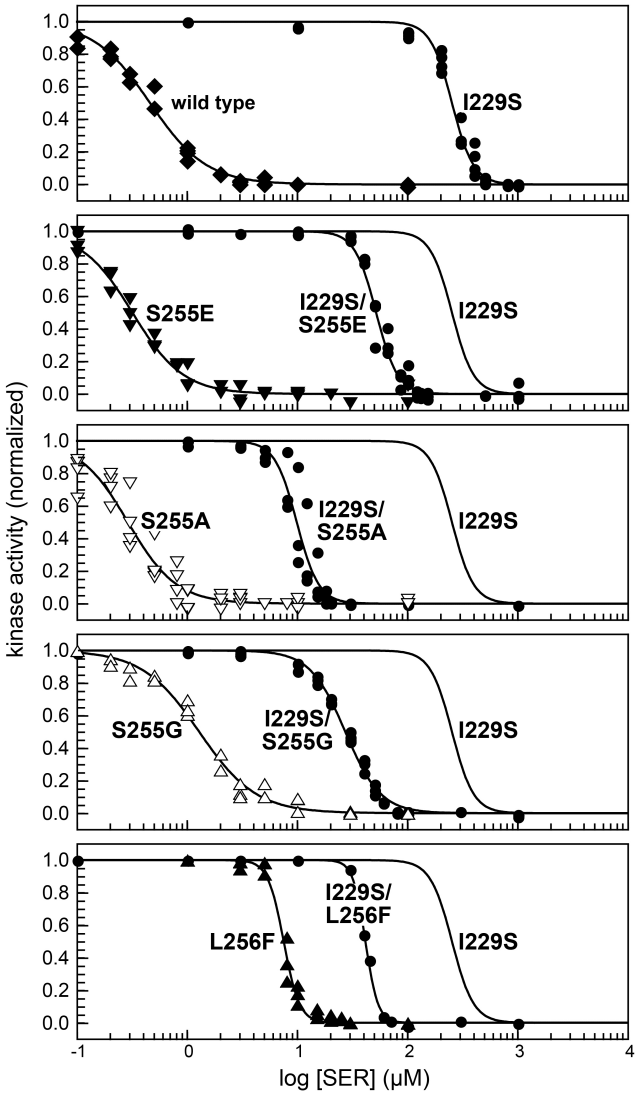

Fig. S4 CheR- and CheB-mediated modifications of mutant Tsr receptors. Plasmid pPA114 derivatives were induced with 0.6 μM salicylate in strains UU2610 (R^- B^-), UU2612 (R^+ B^+), UU2611 (R^- B^+), and UU2632 (R^+ B^-) and Tsr subunits were analyzed by SDS-PAGE. Std: Lane containing wild-type Tsr subunits in EEEEE, QEQEE (dashed lines) and QQQQE modification states as markers. The right side of each gel (not shown) contained combinations of the same size standards for optimizing horizontal orientation. SER: Cell samples untreated (-) or treated (+) with 10 mM serine.

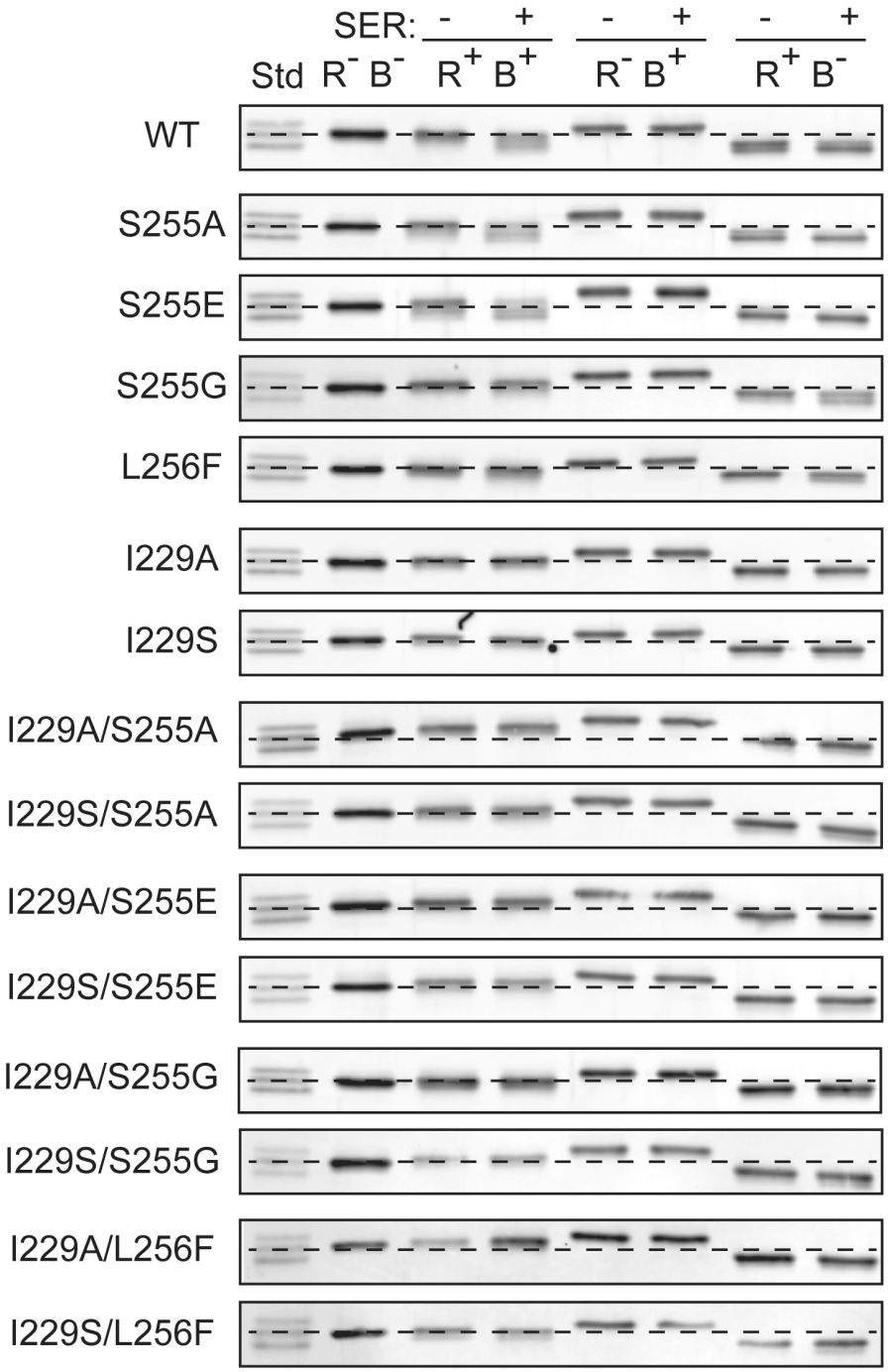

Table S1. Dose-response $K_{1/2}$ values of mutant receptors

host strain:	UU2567 (CheR$^-$ CheB$^-$)					UU2700 (CheR$^+$ CheB$^+$)
modification state:	EEEEE	EEQEE	QEQEE	QQQEE	QQQQE	float
Tsr mutant:						
wild-type	NR-OFF	1.9	17 ± 0.2 [4]	58	164	0.5 ± 0.02 [4]
S255A	NR-OFF	NR-OFF	2.7 ± 0.1 [2]	6.3 ± 0.4 [2]	20 ± 0.8 [2]	0.3 ± 0.01 [4]
S255E	NR-OFF	NR-OFF	NR-OFF [3]	0.4	3.6 ± 0.5 [2]	0.3 ± 0.01 [3]
S255G	33	112	1600 ± 90 [4]	NR-ON	NR-ON	1.3 ± 0.1 [3]
L256F	110	413	NR-ON	NR-ON	NR-ON	7.5 ± 0.1 [3]
I229A	NR-ON	NR-ON	NR-ON [2]	NR-ON	NR-ON	454 ± 6 [3]
I229S	NR-ON	NR-ON	NR-ON [2]	NR-ON	NR-ON	254 ± 6 [4]
I229A/S255A	9100	NR-ON	NR-ON	NR-ON	NR-ON	83 ± 0.9 [4]
I229S/S255A	–	–	NR-ON	–	–	11 ± 1.0 [4]
I229A/S255E	1460	NR-ON	NR-ON	NR-ON	NR-ON	143 ± 2 [4]
I229S/S255E	–	–	NR-ON	–	–	52 ± 3 [3]
I229A/S255G	1100	NR-ON	NR-ON	NR-ON	NR-ON	39 ± 1 [4]
I229S/S255G	–	–	NR-ON	–	–	28 ± 0.7 [4]
I229A/L256F	993	NR-ON	NR-ON	NR-ON	NR-ON	74 ± 1 [4]
I229S/L256F	–	–	NR-ON	–	–	42

Data are means of $K_{1/2}$ values (μM serine) (± standard error) and [number of measurements] (if more than one independent experiment)

NR-OFF: no detectable response to 10 mM serine; little or no kinase activity (see Table S3).

NR-ON: no detectable response to 10 mM serine; high kinase activity (see Table S3).

–: experiment not done

Table S2. Dose-response Hill coefficients of mutant receptors

host strain:	UU2567 (CheR$^-$ CheB$^-$)					UU2700 (CheR$^+$ CheB$^+$)
modification state:	EEEEE	EEQEE	QEQEE	QQQEE	QQQQE	float
Tsr mutant:						
wild-type	NR-OFF	8.7	8.3 ± 0.9 [4]	15	14	1.6 ± 0.1 [4]
S255A	NR-OFF	NR-OFF	3.2 ± 0.2 [2]	17 ± 0.4 [2]	16 ± 10.2 [2]]	2.0 ± 0.1 [4]
S255E	NR-OFF	NR-OFF	NR-OFF [3]	3.6	7.4 ± 4.1 [2]	1.8 ± 0.1 [3]
S255G	22	16	7.0 ± 1.0 [4]	NR-ON	NR-ON	1.9 ± 0.3 [3]
L256F	26	16	NR-ON	NR-ON	NR-ON	6.1 ± 0.6 [3]
I229A	NR-ON	NR-ON	NR-ON [2]	NR-ON	NR-ON	4.5 ± 0.3 [3]
I229S	NR-ON	NR-ON	NR-ON [2]	NR-ON	NR-ON	4.4 ± 0.4 [4]
I229A/S255A	1.4	NR-ON	NR-ON	NR-ON	NR-ON	4.3 ± 0.2 [4]
I229S/S255A	–	–	NR-ON	–	–	4.7 ± 0.3 [3]
I229A/S255E	1.6	NR-ON	NR-ON	NR-ON	NR-ON	4.8 ± 0.3 [4]
I229S/S255E	–	–	NR-ON	–	–	4.6 ± 0.1 [3]
I229A/S255G	10	NR-ON	NR-ON	NR-ON	NR-ON	3.2 ± 0.3 [4]
I229S/S255G	–	–	NR-ON	–	–	2.7 ± 0.1 [4]
I229A/L256F	7.9	NR-ON	NR-ON	NR-ON	NR-ON	5.8 ± 0.4 [4]
I229S/L256F	–	–	NR-ON	–	–	7.6

Data are means of Hill coefficients (± standard error) and [number of measurements] (if more than one independent experiment)

NR-OFF: no detectable response to 10 mM serine; little or no kinase activity (see Table S3).

NR-ON: no detectable response to 10 mM serine; high kinase activity (see Table S3).

–: experiment not done

Table S3. Kinase activities promoted by mutant receptors

host strain:	UU2567 (CheR$^-$ CheB$^-$)					UU2700 (CheR$^+$ CheB$^+$)
modification state:	EEEEE	EEQEE	QEQEE	QQQEE	QQQQE	float
Tsr mutant:						
wild-type	NR / 0.02	1.2 / 1.0	1.0 / 0.90	1.2 / 1.1	1.1 / 0.97	0.21 / –
S255A	NR / 0.04	NR / 0.04	1.1 / 0.94	1.1 / 0.95	1.0 / 0.95	0.14 / –
S255E	NR / 0.03	NR / 0.03	NR / 0.05	0.71 / 0.75	0.75 / 0.75	0.18 / –
S255G	1.3 / 1.3	1.2 / 1.2	0.97 / 0.97	*0.10* / 1.1	*0.03* / 0.78	0.69 / –
L256F	1.2 / 1.2	1.1 / 1.1	*0.06* / 1.0	NR / 0.97	NR / 0.99	1.4 / –
I229A	*0.14* / 1.1	*0.06* / 1.1	*0.12* / 1.1	*0.12* / 1.1	*0.08* / 0.97	1.3 / –
I229S	*0.05* / 0.90	*0.02* / 0.96	*0.04* / 0.93	*0.04* / 0.53	NR / 0.58	0.85 / –
I229A/S255A	0.76 / 0.89	*0.08* / 1.0	*0.05* / 0.82	*0.03* / 0.99	*0.03* / 0.67	1.0 / –
I229S/S255A	– / –	– / –	*0.05* / 0.91	– / –	– / –	0.87 / –
I229A/S255E	*0.45* / 0.89	*0.07* / 1.0	*0.04* / 0.71	*0.04* / 0.95	*0.03* / 0.91	0.71 / –
I229S/S255E	– / –	– / –	*0.04* / 0.70	– / –	– / –	1.1 / –
I229A/S255G	0.91 / 0.86	*0.04* / 0.90	NR / 0.90	*0.03* / 0.71	NR / 0.86	0.66 / –
I229S/S255G	– / –	– / –	*0.03* / 0.78	– / –	– / –	1.0 / –
I229A/L256F	0.73 / 0.74	*0.07* / 0.85	*0.03* / 0.68	*0.03* / 0.47	NR / 0.66	0.82 / –
I229S/L256F	– / –	– / –	*0.05* / 0.98	– / –	– / –	1.4 / –

Kinase activities are relative to that of wild-type Tsr in the QEQEE modification state. Values to the left of the backslash are derived from FRET responses to saturating serine stimuli; values to the right are derived from FRET changes elicited by 3 mM KCN treatment. Italicized values are based on non-saturating serine responses.

NR: no detectable response to 10 mM serine

–: experiment not done

Table S4. Comparison of mutant receptor response parameters in various host strains

host strain:	UU2567	UU2699	UU2697	UU2700	UU2612
adaptation enzyme(s):	none	CheB	CheR	CheR & CheB	CheR & CheB
modification state(s):	QEQEE	EEEEE... ...QEQEE	QEQEE... ...QE_mQE_{mEm}	float	serine threshold on soft agar (μM)
Tsr mutant:					
wild-type	17 ± 0.2; 8.3 ± 0.9	NR-OFF	51; 2.2	0.5 ± 0.02; 1.6 ± 0.1	4
S255A	2.7 ± 0.1; 3.2 ± 0.2	NR-OFF	8.6 ± 1.0; 4.2 ± 0.6	0.3 ± 0.01; 2.0 ± 0.1	4
S255E	NR-OFF	NR-OFF	2.6 ± 0.2; 5.7 ± 1.1	0.3 ± 0.01; 1.8 ± 0.1	4
S255G	1600 ± 90; 7.0 ± 1.0	22 ± 2.4; 12 ± 3.4	NR-ON	1.3 ± 0.1; 1.9 ± 0.3	20
L256F	NR-ON	130; 9.4	NR-ON	7.5 ± 0.1; 6.1 ± 0.6	100
I229A	NR-ON	NR-ON	NR-ON	454 ± 6; 4.5 ± 0.3	NR
I229S	NR-ON	NR-ON	NR-ON	254 ± 6; 4.4 ± 0.4	NR
I229A/S255A	NR-ON	4100	NR-ON	83 ± 0.9; 4.3 ± 0.2	~670
I229S/S255A	NR-ON	230	NR-ON	11 ± 1.0; 4.7 ± 0.3	~670
I229A/S255E	NR-ON	22,000	NR-ON	143 ± 2; 4.8 ± 0.3	~670
I229S/S255E	NR-ON	2700	NR-ON	52 ± 3; 4.6 ± 0.1	~670
I229A/S255G	NR-ON	1000	NR-ON	39 ± 1; 3.2 ± 0.3	~670
I229S/S255G	NR-ON	2000	NR-ON	28 ± 0.7; 2.7 ± 0.1	~670
I229A/L256F	NR-ON	1000	NR-ON	74 ± 1; 5.8 ± 0.4	~670
I229S/L256F	NR-ON	1100	NR-ON	42; 7.6	~670

Values are means (± standard errors) of $K_{1/2}$ (μM serine); Hill coefficient.

NR-OFF: no detectable response to 10 mM serine; little or no kinase activity.

NR-ON: no detectable response to 10 mM serine; high kinase activity.